# Modification of Multiwall Carbon Nanotubes by *Grafting from* Controlled Polymerization of Styrene: Effect of the Characteristics of the Nanotubes

**JULIO ALBUERNE, ADRIANA BOSCHETTI-de-FIERRO, VOLKER ABETZ**

Institute of Polymer Research, GKSS Research Centre Geesthacht GmbH, Max-Planck-Str. 1, Geesthacht 21502, Germany

Received 26 September 2009; revised 5 February 2010; accepted 6 February 2010
DOI: 10.1002/polb.21992
Published online in Wiley InterScience (www.interscience.wiley.com).

**ABSTRACT**: Linear polystyrene chains were grown from the convex surface of two commercially available multiwall carbon nanotubes (MWCNTs) with similar diameter but different lengths. The MWCNTs were supplied from Bayer Material Science® (purity >95%, external diameter = 13–16 nm, length = 1–10 $\mu$m, denoted $MWCNT_{BMS}^{95}$) and FutureCarbon GmbH (purity >99%, external diameter = 15 nm, length = 5–50 $\mu$m, denoted $MWCNT_{FC}^{99}$). The MWCNTs were oxidized with nitric acid, consecutively reacted with thionyl chloride, glycol or poly(ethylene glycol), 2-bromo-2-methylpropionyl bromide and finally with styrene under atom transfer radical polymerization (ATRP) conditions. The content of polystyrene grafted from the surface of the MWCNTs can be controlled by adjusting the molecular weight of the poly(ethylene glycol), the initiator concentration and the monomer to carbon nanotube weight ratio. Under comparable experimental conditions, a higher amount of polystyrene is grafted from the $MWCNT_{BMS}^{95}$ than from $MWCNT_{FC}^{99}$. The difference in dimensions and the state of aggregation of the carbon nanotubes influence the *grafting from* polymerization reactions, where relative shorter and tightly aggregated carbon nanotubes promote higher polymerizations yields than longer and less aggregated carbon nanotubes. The increase of the viscosity of the carbon nanotube dispersion decreases the polymer grafting content. © 2010 Wiley Periodicals, Inc. J Polym Sci Part B: Polym Phys 48: 1035–1046, 2010

**KEYWORDS**: atom transfer radical polymerization (ATRP); carbon nanotubes; grafting from polymerization; multiwall carbon nanotubes; polystyrene; thermogravimetric analysis (TGA)

**INTRODUCTION** The incorporation of carbon nanotubes in polymer matrices has become a challenge during the past decade.[1] Carbon nanotubes consist of graphene sheets rolled up into a cylindrical shape. They are classified depending on the number of graphene layers. Their dimensions range up to few hundred nanometers in diameter and tens of micrometers in length.[2,3] They have outstanding mechanical, electrical, and thermal properties, which have inspired the design of a new generation of light weight materials,[1,4,5] or even their use as biosensors or biocarriers,[6–9] although their biocompatibility is still questionable.[10–13]

One of the drawbacks of the incorporation of this type of nanofiller in polymer matrices is its tendency to aggregate due to the strong $\pi$–$\pi$ stacking interactions between graphene sheets. Different strategies have been used to reduce the size of the aggregates or to improve the dispersion of individual carbon nanotubes. Sonication, centrifugation, calendaring, or intense stirring have shown promising results on single (SWCNT), double (DWCNT), and multiwall (MWCNT) carbon nanotube dispersions in solvents and different polymer matrices.[4,5,14–16] Other approaches aim for the tuning of the surface of carbon nanotubes through the physisorption of surfactants and polymers,[17] or through the direct functionalization on the surface of the nanoparticle. Tasis et al.[18] have presented a review related with the chemistry of carbon nanotubes. They have categorized the modification of carbon nanotubes into three groups: the endohedral filling of their inner empty cavity, the noncovalent adsorption or wrapping of various functional molecules, and the covalent attachment of small molecules or polymer chains through reactions onto the $\pi$-conjugated skeleton of the carbon nanotubes. In the first case, the research has been focused on the production of nanowires or on the storage of liquid fuels. The works have been mainly related with the encapsulation of fullerenes, metalofullerenes, metal salts (subsequently reduced to metals), metal oxides, inorganic salts, and biomolecules in SWCNTs and MWCNTs. There are also examples of conjugated polymers that have the ability of wrapping the carbon nanotubes, usually, with a helical conformation. There are two main approaches for the covalent attachment of polymers on carbon nanotubes, known as *grafting onto* and *grafting from*. The former consists on attaching polymer chains onto the surface of carbon nanotubes through the reaction with end or side functionalized polymer chains. Unfortunately, the efficiency of the grafting reactions is sometimes inaccurate due to the presence of nongrafted polymer.[19–21] The *grafting from* relies on the polymerization from the carbon nanotubes through the immobilization of a polymer precursor at the particle

Correspondence to: V. Abetz (E-mail: volker.abetz@gkss.de)
Journal of Polymer Science: Part B: Polymer Physics, Vol. 48, 1035–1046 (2010) © 2010 Wiley Periodicals, Inc.



10990488, 2010, 10, Downloaded from https://onlinelibrary.wiley.com/doi/10.1002/polb.21992 by Farrah Choudry - Test , Wiley Online Library on [21/12/2022]. See the Terms and Conditions (https://onlinelibrary.wiley.com/terms-and-conditions) on Wiley Online Library for rules of use; OA articles are governed by the applicable Creative Commons License



Samsung Ex. 1009, Page 1 of 12
Samsung Electronics Co., Ltd., et al. v. Molecular Rebar Design, LLC
IPR2025-00358

surface.[18] In this case, a series of prefunctionalization reactions are required to covalently anchor groups capable to initiate the polymerization. However, the concentration of initiator groups and the final characteristics of the grafted polymer (i.e., molecular weight and weight content) can be tuned by the adjustment of the prefunctionalization reactions. The most versatile technique used on the grafting of polymer from carbon nanotubes (and other substrates) is the controlled radical polymerization[8,22–41] because a broad number of monomers is available, it generally does not require an elaborated setup, and it accepts some level of impurities on the carbon nanotubes and the reaction system. There are diverse references regarding the grafting from carbon nanotubes where the control on the polymerization is achieved by adjusting the concentration of monomer, initiator, or deactivator.[8,28,31,32,42] However, to the author's knowledge, the influence of the carbon nanotubes on the reactions has not been discussed so far. In comparison, for silica nanospheres their influence has been previously studied, where the success of the grafting polymerization was discussed as a function of the sphere diameter,[43] and the characteristics of the initiator groups attached at the surface.[44] The characteristics of the carbon nanotubes and how they could affect the surface functionalization has not been discussed until now, mainly because they vary depending on the supplier and the method of synthesis. Here, a comparison between two commercially available multiwall carbon nanotubes (MWCNTs) subjected to functionalization reactions and their influence on the *grafting from* of styrene is presented for the first time. In this work, a multistep functionalization procedure was chosen, where the carbon nanotubes have been characterized after each reaction step as a function of their characteristics and behavior after each reaction. Finally, the factor that controls the content of grafted polystyrene has been tuned and compared for the studied nanoparticles.

## EXPERIMENTAL

### Materials

MWCNTs were obtained from Bayer MaterialScience® (Baytubes, purity >95%, internal mean diameter = 4 nm, external mean diameter = 13–16 nm, length = 1–10 $\mu$m, number of walls = 3–15, denoted $MWCNT_{BMS}^{95}$) and FutureCarbon GmbH (purity >99%, internal mean diameter = 6 nm, external mean diameter = 15 nm, length = 10–50 $\mu$m, number of walls = 10, denoted $MWCNT_{FC}^{99}$). In the notation used here, that is, $MWCNT_x^y$, the subscript x indicates the MWCNT manufacturer and the superscript y the carbon purity of the nanotube. Nitric acid ($HNO_3$, 65% v/v), thionyl chloride ($SOCl_2$, ≥99%), ethylene glycol (EG), poly(ethylene glycol) of 200 g mol $^{1}$ and 400 g mol $^{1}$ ($PEG_{200}$ and $PEG_{400}$, respectively), 2-bromo-2-methylpropionyl bromide (2BriBr, 99%), triethyl amine ($Et_3N$, ≥99.5%), dimethyl amino pyridine (DMAP, 97%), copper(I) bromide (CuBr, 99%), *N,N,N′,N′,N*-pentamethyl diethylenetriamine (PMDETA, 97%), tetrahydrofurane (THF), and anisole were used as received. Chloroform ($CHCl_3$) and styrene (S) were dried over calcium hydride ($CaH_2$) and distilled before use. All the reagents were purchased from Aldrich.

### Oxidation of the MWCNTs

In a typical experiment, 1 g of $MWCNT_x^y$ was dispersed in 40 mL of $HNO_3$ in a round bottom flask. After 30 min of sonication at room temperature, the system was heated at 65 °C for 48 h under continuous stirring. The dispersion was then filtered and washed with copious amounts of distilled water until the pH reached constant values. Finally, the oxidized carbon nanotubes were dried at 60 °C under vacuum for 72 h.

### Acid to Acid Chloride Conversion and Esterification I: Glycol Spacer

The oxidized MWCNTs (400 mg) were chlorinated in the presence of $SOCl_2$ (28 mL) for 24 h at 65 °C. After reaction, the dispersion was generously washed with THF, filtered, and dried at ambient temperature overnight. The acyl or alkyl chloride functionalized MWCNTs were heated with different amounts of EG or PEG at 120 °C for 48 h. The hydroxyl decorated carbon nanotubes were passed through a Teflon® membrane (0.2 $\mu$m pore size), washed with THF, and dried for 48 h at ambient temperature. The products were repeatedly dispersed, filtered, and dried. Details of the reaction can be appreciated in Table 1.

### Anchoring of Initiator Groups

The functionalization with initiator groups suitable for the grafting of styrene was done following the work of Kong et al.[31] In a typical reaction (see Table 1, entry 1), hydroxyl decorated MWCNTs (150 mg) were dispersed in $CHCl_3$ (19.2 mL) with a catalytic amount of $Et_3N$ (228 $\mu$L) and DMAP (29 $\mu$L). The system was immersed in a sonication bath for 10 min under Ar flow. Then, the dispersion was cooled down in an ice bath and thrice vacuum filled with Ar. A diluted solution of 2BriBr (210 $\mu$L) in $CHCl_3$ (2.4 mL) was added drop wise for ~1 h. The reaction was kept in the ice bath for 3 h and after that at ambient temperature for 48 h. After reaction, the carbon nanotubes grafted with initiator groups were passed through a Teflon® membrane and washed with copious amounts of $CHCl_3$. The carbon nanotubes were redispersed, filtered, and dried three times. Elemental analysis (atomic %): C, 92.25; H, 0.49; Br, 0.57. The notation used is $MWCNT_x^y$-Br, where the Br indicates the anchoring of the initiator. Details of the reaction can be appreciated also in Table 1.

### *Grafting from* Styrene Under Atom Transfer Radical Polymerization

In a Schlenk tube, $MWCNT_{BMS}^{95}$-Br or $MWCNT_{FC}^{99}$-Br, 0.7 mol % of CuBr (respect to the monomer) and S were dispersed in anisole (4 vol % respect to the monomer) under Ar flow for 60 min. After three freeze-pump-thawed cycles, 0.7 mol % of PMDETA (respect to the monomer) was added and the tube transferred into an oil bath at 90 °C. When the reaction was completed, the system was diluted in toluene and precipitated in methanol. The precipitated sample was filtered using a Teflon® membrane and dried for 48 h. After drying, the polymer grafted carbon nanotubes were again



10990488, 2010, 10, Downloaded from https://onlinelibrary.wiley.com/doi/10.1002/polb.21992 by Farrah Choudry - Test , Wiley Online Library on [21/12/2022]. See the Terms and Conditions (https://onlinelibrary.wiley.com/terms-and-conditions) on Wiley Online Library for rules of use; OA articles are governed by the applicable Creative Commons License



Samsung Ex. 1009, Page 2 of 12
Samsung Electronics Co., Ltd., et al. v. Molecular Rebar Design, LLC
IPR2025-00358

10990488, 2010, 10, Downloaded from https://onlinelibrary.wiley.com/doi/10.1002/polb.21992 by Farrah Choudry - Test , Wiley Online Library on [21/12/2022]. See the Terms and Conditions (https://onlinelibrary.wiley.com/terms-and-conditions) on Wiley Online Library for rules of use; OA articles are governed by the applicable Creative Commons License

**TABLE 1** Experimental Conditions Used for the Esterification with Glycols and 2BriBr of $MWCNT_{BMS}^{95}$ and $MWCNT_{FC}^{99}$

| | | Esterification I (EG or PEG)[a] | | Esterification II Initiator Anchoring | | |
|---|---|---|---|---|---|---|
| Entry | Sample | Type[a] | [Glycol] (mol $g^{-1}$)[b] | [2BriBr] ($\mu$L $mg^{-1}$)[c] | [MWCNT] (mg $mL^{-1}$)[d] | [Br] (mmol $g^{-1}$)[e] |
| 1 | $MWCNT_{FC}^{99}$-$Br^1$ | EG | 1.3 | 1.4 | 6.5 | 0.07 |
| 2 | $MWCNT_{FC}^{99}$-$Br^2$ | EG | 1.3 | 2.7 | 6.9 | 0.13 |
| 3 | $MWCNT_{FC}^{99}$-$Br^3$ | $PEG_{200}$ | 1.3 | 2.7 | 6.9 | 0.22 |
| 4 | $MWCNT_{FC}^{99}$-$Br^4$ | $PEG_{400}$ | 1.3 | 5.4 | 6.9 | 0.24 |
| 5 | $MWCNT_{FC}^{99}$-$Br^5$ | $PEG_{400}$ | 0.6 | 2.7 | 6.0 | 0.04 |
| 6 | $MWCNT_{FC}^{99}$-$Br^6$ | $PEG_{400}$ | 1.3 | 2.7 | 6.9 | 0.14 |
| 7 | $MWCNT_{FC}^{99}$-$Br^7$ | $PEG_{200}$ | 1.3 | 2.7 | 6.9 | 0.08 |
| 8 | $MWCNT_{BMS}^{95}$-$Br^1$ | EG | 1.3 | 1.4 | 15.6 | 0.08 |
| 9 | $MWCNT_{BMS}^{95}$-$Br^2$ | EG | 1.3 | 2.7 | 16.0 | 0.62 |
| 10 | $MWCNT_{BMS}^{95}$-$Br^3$ | $PEG_{200}$ | 1.3 | 1.4 | 15.7 | 0.36 |
| 11 | $MWCNT_{BMS}^{95}$-$Br^4$ | $PEG_{400}$ | 1.3 | 1.4 | 15.6 | 0.15 |

[a] EG: ethylene glycol; $PEG_{200}$ and $PEG_{400}$: poly(ethylene glycol) of average number molecular weight of 200 g mol $^{1}$ and 400 g mol $^{1}$, respectively.
[b] Relation between mole of ethylene glycol or poly(ethylene glycol) and MWCNT (g) used.
[c] Concentration of 2-bromo-2-methylpropionyl bromide (2BriBr, $\mu$L) respect to MWCNT (mg).
[d] Relation between MWCNT (mg) and $CHCl_3$ (mL) used during the reaction.
[e] [Br] determined by elemental analysis.

dispersed in $CHCl_3$ for 24 h, filtered, and dried. This procedure was repeated until no traces of polymer were collected from the filtered solution by precipitation in methanol. The polystyrene grafted carbon nanotubes are denoted $PS_w^qMWNCNT_x^y$, where the subscript *w* represents the weight percent of polystyrene grafted, and the superscript q represents the molecular weight of the grafted polymer (in kg mol $^{1}$).

### Characterization

Fourier transform infrared spectra (FTIR) were conducted on a Bruker Equinox 55. The samples were dispersed in potassium bromide (KBr) and compressed as disks. Thermal gravimetric analyses (TGA) were carried out on a Netzsch TG209 F1 Iris under constant Ar flow, at a rate of 20 °C min $^{1}$. Scanning electron microscopy (SEM) studies were performed on a Zeiss LEO Gemini 1550VP (1 kV). Samples were carefully glued on conductive tape and sputtered with a fine Au/Pd layer. Transmission electron microscopy (TEM) observations were done on a Fei Tecnai $G^2$ F20 (200 kV). The samples were dispersed in $CHCl_3$ or THF and dropped on grids. Scanning force microscopy (SFM) images were taken on a "Veeco" MultimodeTM AFM (NanoScope IV controller) operating in tapping mode at ambient temperature. Silicon TM AFM tips (model MPP-12100) with a free resonance of 150 kHz and spring constant of 5 N m $^{1}$ were used. The carbon nanotubes were dispersed in $CHCl_3$ (5% w/v) for 24 h at ambient temperature. After 24 h, the dispersions were homogenized for 1 min with an ultrasonic probe (Bandelin SONOPULS®, frequency = 20 kHz) and one drop (5 $\mu$L) was placed on a cleaned polished silicon wafer. The silicon wafers were previously cleaned in a water-saturated UV-ozone atmosphere for at least 24 h. The viscosities of the carbon nanotubes dispersions before and after the oxidation reactions were measured using a Brookfield R/S rheometer. The experiments were performed at a constant rate (500 s $^{1}$) for 2 min in a plate/plate geometry (C75-1). The carbon nanotubes (1% w/v) were dispersed in ethylene glycol for 24 h at ambient temperature. Before the measurements, the dispersions were then homogenized for 5 min with an ultrasonic probe (Bandelin SONOPULS®, 20 kHz, amplitude = 50%).

## RESULTS AND DISCUSSION

### Oxidation of the MWCNTs

The scheme of the modification of MWCNTs is shown in Figure 1. A similar procedure has been adopted previously by other groups.[31,39,42] The reactions that lead to anchoring of initiator groups able to initiate the polymerization of styrene are based on well-known organic chemistry reactions. The first step implies the oxidation of the pristine MWCNTs with $HNO_3$. The FTIR spectra of the pristine and oxidized MWCNTs can be appreciated in Figure 2. Many authors attribute the signals between 1650 cm $^{1}$ and 1540 cm $^{1}$ to the C=C stretching mode of the aromatic ring.[45–47] Around 1460 cm $^{1}$, the C—H bending alkyl vibrations can be observed. Besides these signals, other features in the pristine MWCNTs are interesting. A clear C—H stretching vibration in the vicinity of a carboxylic group (~1430 cm $^{1}$) and a rocking vibration (~1380 cm $^{1}$) could indicate the presence of quinones and aldehydes, respectively. The C=O vibration in both cases might be overlapped with the stretching mode of the aromatics. Another feature around 1160 cm $^{1}$ is related with the C—O—C stretching from aromatic esters. The described bands show that the MWCNT skeleton is not just composed of crystalline graphene layers but have also defects coming from the synthesis or the rest of catalyst. These imperfections might have consequences on the properties of the MWCNTs, however, they may also represent an





Samsung Ex. 1009, Page 3 of 12
Samsung Electronics Co., Ltd., et al. v. Molecular Rebar Design, LLC
IPR2025-00358

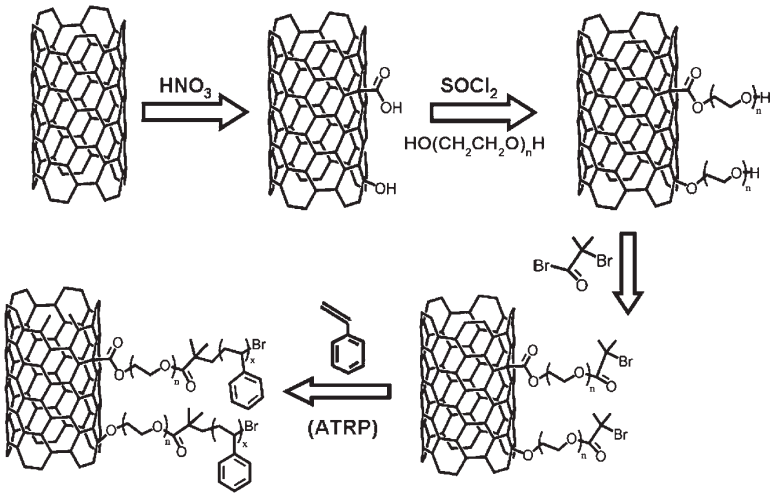


**FIGURE 1** Schematic representation of the surface modification reactions carried out on MWCNTs.

advantage if reactions on these "weak points" can improve the dispersion of the MWCNTs in solvents or polymers. After oxidation, a C=O stretching vibration related with esters is easily identified for the $MWCNT_{FC}$[99] (1710 cm $^{1}$).[48] In the case of the $MWCNT_{BMS}$[95], the C=O vibration is located at a lower wavenumber (broad peak) that would indicate the presence of carboxylic acid,[49] and a relative increase in the intensity at 1575 cm $^{1}$ is observed. This signal might be related with a keto-enol tautomerism. One interesting change due to the oxidation reaction is the appearance of a strong signal in MWCNTs from both suppliers around 1380 cm $^{1}$. The assignment could be related again with the C—H rocking vibration of aldehydes, but this would imply a stronger signal at around 1700–1650 cm $^{1}$, which is not observed. A second and more probable explanation could be the formation of phenols which present such strong signal due to the combination of O—H and C—O deformation vibrations. The oxidation favors the formation of phenol groups in MWCNTs from both suppliers; ester groups seem more favorable in case of the $MWCNT_{FC}$[99], whereas in the case of the $MWCNT_{BMS}$[95] the presence of ketones and carboxylic acid groups is predominant. The formation of carbonyl and hydroxyl groups at MWCNTs after the reaction with $HNO_3$ (and other carbonaceous fibers)[50] has been widely described by other groups using different characterization techniques,[48,51–55] where a qualitative increase in FTIR signal intensity in the region of the carbonyl or hydroxyl groups is associated to a discrete increase on the concentration of oxygen atoms at the surface of the carbon nanotubes. This increment has proven to be satisfactory for further reactions of the carbon nanotubes with small molecules[51] or with polymer chains.[52,56]

It is known that, to obtain high concentrations of carboxylic acid groups (or their derivatives) on carbon nanotubes, treatments more aggressive than the one used here are required, such as combinations of $HNO_3$ with stronger acids (like sulfuric acid) or air oxidation at high temperatures.[50,54,57,58] Such treatments lead to the destruction of the graphitic structure, reduction on the carbon nanotube length, disaggregation of nanotube bundles, and improvement of the dispersion of the carbon nanotubes in organic solvents. The aim of the chosen acid treatment was to preserve the carbon nanotubes by attacking defects already present in the structure and to dissolve the catalysts and the synthesis by-products (e.g., amorphous carbon), without cutting the length of the nanotubes or loosing any of the walls.[48] Figure 3 shows transmission electron microscope images of the pristine and oxidized $MWCNT_{BMS}$[95]. The rest of catalyst or amorphous carbon is evidenced in Figure 3(a) on the left side of the

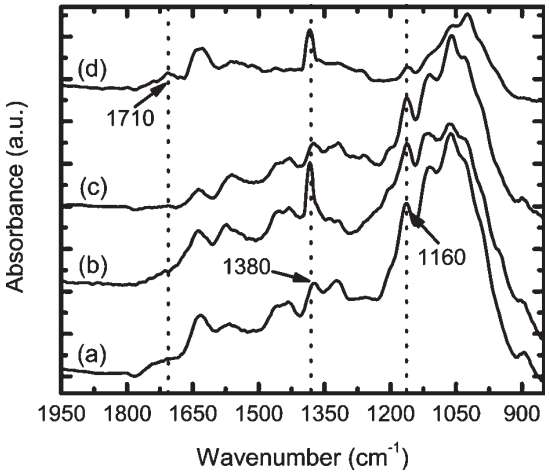


**FIGURE 2** Fourier transform infrared spectra of MWCNTs from different sources before and after the oxidation reaction: (a) pristine and (b) oxidized $MWCNT_{BMS}$[95], (c) pristine and (d) oxidized $MWCNT_{FC}$[99].



10990488, 2010, 10, Downloaded from https://onlinelibrary.wiley.com/doi/10.1002/polb.21992 by Farrah Choudry - Test , Wiley Online Library on [21/12/2022]. See the Terms and Conditions (https://onlinelibrary.wiley.com/terms-and-conditions) on Wiley Online Library for rules of use; OA articles are governed by the applicable Creative Commons License



Samsung Ex. 1009, Page 4 of 12
Samsung Electronics Co., Ltd., et al. v. Molecular Rebar Design, LLC
IPR2025-00358

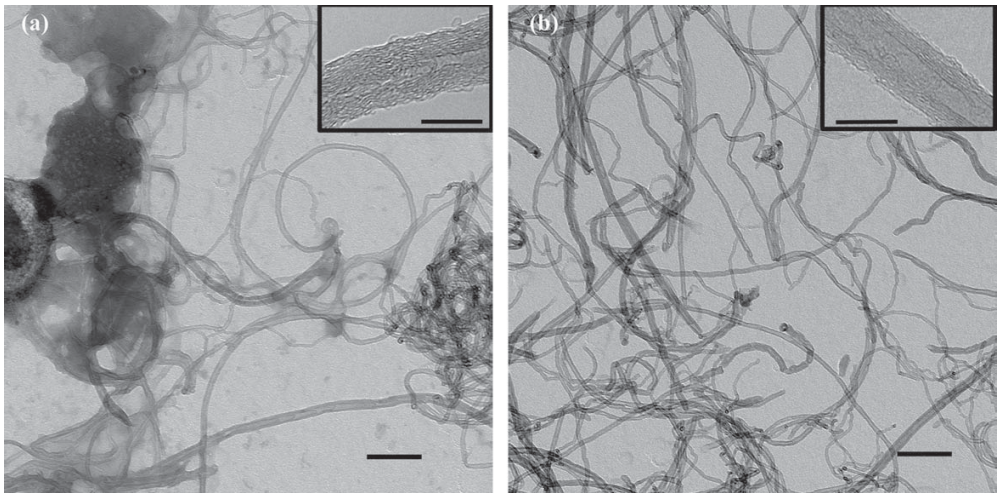


**FIGURE 3** Transmission electron micrographs of (a) pristine and (b) oxidized $MWCNT_{BMS}$[95]. Scale bar = 100 nm, insert = 10 nm.

image. These amorphous aggregates were not found on any of the images after the treatment with $HNO_3$. Zhang et al.[53] also reported the decomposition of the catalyst or amorphous carbon under comparable reaction conditions. In addition, TEM images show that the numbers of walls are preserved (see inserts in Fig. 3). In the case of the $MWCNT_{FC}$[99], catalyst residues were not appreciated in the pristine sample during the observations (results not shown). Some pioneering works have proposed correlation models between the nanotubes length against reaction time for different oxidation systems on SWCNT.[57,59] Unfortunately, these results cannot be directly correlated to the ones presented here because the oxidation depends on factors related with the number of walls, purity, synthesis process, and source of the carbon nanotubes.[50] A systematic study is required to understand the effect of the oxidation on identical MWCNTs exposed to mild and aggressive oxidation conditions.

### Acid to Acid Chloride Conversion and Esterification I: Glycol Spacer

Further reaction between the oxidized carbon nanotubes and thionyl chloride leads to the formation of alkyl and acyl chloride groups. Experimental and theoretical evidences have shown that carbon nanotubes could also absorb thionyl chloride and the presence of moisture gives rise to by-products that could form C—Cl bonds on the structural defects.[60] The acyl or alkyl chloride groups are highly reactive and can further form esters or ethers, respectively, in the presence of an alcohol. Glycols of different molecular weights were used in this work. These $\alpha,\omega$-dihydroxy-functionalized telechelics will be used as spacers between the carbon nanotubes and the initiator moieties necessary for the *grafting from* of styrene. While increasing the glycol molecular weight from 62 g mol $^{1}$ (ethylene glycol) to 400 g mol $^{1}$, the weight loss between 100 °C and 500 °C (determined by thermal gravimetric analysis) increases from ~5% to more than 12%, in the case of the $MWCNT_{FC}$[99] and from 5 to 18% in the case of the $MWCNT_{BMS}$[95], as can be appreciated in Figure 4.

The MWCNT source also has an effect on the reaction product; since it was observed that the grafting content of ethylene glycol on $MWCNT_{BMS}$[95] is almost the double of the content obtained on $MWCNT_{FC}$[99]. On the one hand, the concentration of reactive groups on $MWCNT_{BMS}$[95] and $MWCNT_{FC}$[99] could explain the difference in grafting efficiency; however, the characterization techniques available for the determination of the concentration are still not reliable. On the other hand, the difference in grafting could also be attributed to the differences in the dimension of the carbon nanotube and the quality of the dispersion during the reaction. The contour length of the pristine and the oxidized MWCNTs were examined by scanning force microscopy (SFM). The distribution of the MWCNTs contour lengths can

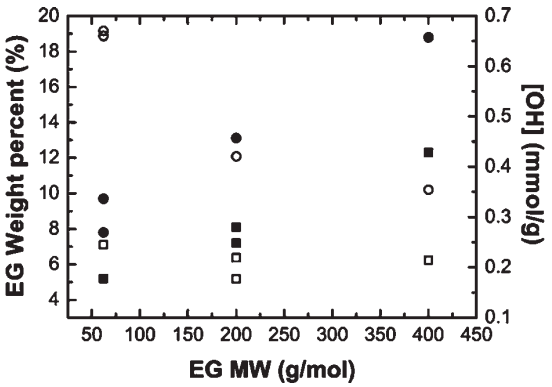


**FIGURE 4** Glycol grafting content (left axes, filled symbols) and concentration of hydroxyl groups (right axes, open symbols) versus glycol molecular weight for $MWCNT_{BMS}$[95] (●, ○) and $MWCNT_{FC}$[99] (■, □).



10990488, 2010, 10, Downloaded from https://onlinelibrary.wiley.com/doi/10.1002/polb.21992 by Farrah Choudry - Test , Wiley Online Library on [21/12/2022]. See the Terms and Conditions (https://onlinelibrary.wiley.com/terms-and-conditions) on Wiley Online Library for rules of use; OA articles are governed by the applicable Creative Commons License



Samsung Ex. 1009, Page 5 of 12
Samsung Electronics Co., Ltd., et al. v. Molecular Rebar Design, LLC
IPR2025-00358

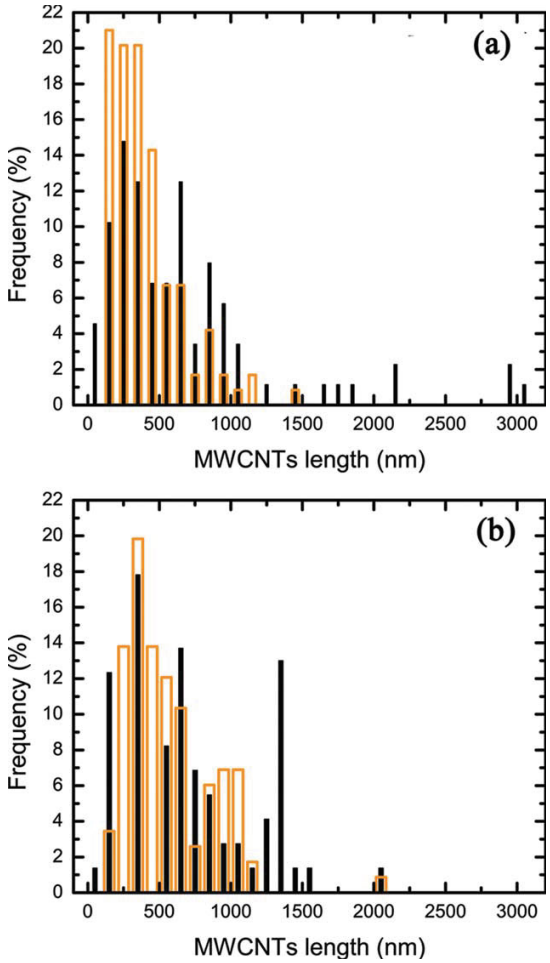


**FIGURE 5** Carbon nanotube length distribution (nm) of (a) pristine MWCNTs and (b) oxidized MWCNTs, calculated from SFM phase images. Filled bars (black) correspond to $MWCNT_{BMS}^{95}$ and contour bars (orange) correspond to $MWCNT_{FC}^{99}$.

be appreciated in Figure 5. Approximately one hundred independent length measurements were done on each case, from different positions on several silicon wafers.

Although the reported information in the technical data sheets of the products indicates that the $MWCNT_{BMS}^{95}$ are on average shorter than the $MWCNT_{FC}^{99}$, the results in Figure 5 show the contrary. The length distributions of the pristine carbon nanotubes are 370 ± 60 nm and 225 ± 30 nm, for $MWCNT_{BMS}^{95}$ and $MWCNT_{FC}^{99}$, respectively. It has to be pointed out that just the carbon nanotubes dispersed on the silicon wafers were taken into account for the measurements, longer carbon nanotubes than the ones measured could not be identified on any of the images taken. Longer carbon nanotubes are probably present on the samples included inside the aggregates. The ultrasonic probe was used to disaggregate the carbon nanotubes before dropping the dispersion on the silicon wafer. The ultrasonic treatment could induce the cleavage of the carbon nanotubes, especially if the graphitic structure has defects. In any case, comparison can be made between the $MWCNT_{BMS}^{95}$ and the $MWCNT_{FC}^{99}$ because the carbon nanotubes were dispersed under the same conditions. After the acid treatment, the population of carbon nanotubes with shorter lengths decreases in both cases, which evidences that the $HNO_3$ is also able to disrupt the carbon nanotubes. The carbon nanotube length distribution is slightly shifted to higher values after the acid treatment, which could indicate that the reaction unbundles longer carbon nanotubes from the aggregates.

Although the SFM measurements give an indication of the length of the isolate carbon nanotubes, the viscosity of the dispersion of carbon nanotubes could give evidences of the state of aggregation of the nanoparticles. Table 2 shows the viscosity of the dispersion of MWCNTs in ethylene glycol before and after the acid treatment. The viscosity of the MWCNTs dispersions in ethylene glycol increases after the acid treatment. The viscosity of the dispersion of the $MWCNT_{FC}^{99}$ is more than two times higher than the $MWCNT_{BMS}^{95}$. This difference could be associated to the structure of the aggregates. It is known that the synthesis process of the $MWCNT_{BMS}^{95}$ leads to the formation of highly bundled nanoparticles, whereas the synthesis of the $MWCNT_{FC}^{99}$ leads to more loose aggregates. The results obtained could indicate that the highly aggregated MWCNTs have a minor influence on the viscosity of the dispersion whereas, on the contrary, the loose aggregate structure increases the relative viscosity of the dispersion. The increase in viscosity can be associated with the disaggregation of the MWCNTs that leads to the presence of longer carbon nanotubes or looser aggregates in the dispersion. It has to be mentioned that the error on the measurements increases for the oxidized carbon nanotubes. This might indicate that the treatment on the nanoparticles depends on the state of the particle in the dispersion and the experimental conditions used. For example, it could be expected that the $HNO_3$ oxidize faster nanoparticles with more structural defects or might easily unbundles loose agglomerate than compact ones. Also, the variation of the conditions of the acid treatment could lead to the homogenization of the nanoparticles (e.g., dispersion of isolate particles or homogeneous size of aggregates), however, the conditions used on this work were meant to evaluate the difference between carbon

**TABLE 2** Viscosity of the Dispersion of MWCNTs in Ethylene Glycol (1% w/v)

| Sample | Description | $\eta$ (MPa s) |
|---|---|---|
| Ethylene glycol | | 17 ± 1 |
| $MWCNT_{BMS}^{95}$ | Pristine | 63 ± 1 |
| | Oxidized | 75 ± 10 |
| $MWCNT_{FC}^{99}$ | Pristine | 154 ± 1 |
| | Oxidized | 280 ± 70 |

Values obtained at 500 $s^{-1}$.



10990488, 2010, 10, Downloaded from https://onlinelibrary.wiley.com/doi/10.1002/polb.21992 by Farrah Choudry - Test , Wiley Online Library on [21/12/2022]. See the Terms and Conditions (https://onlinelibrary.wiley.com/terms-and-conditions) on Wiley Online Library for rules of use; OA articles are governed by the applicable Creative Commons License



Samsung Ex. 1009, Page 6 of 12
Samsung Electronics Co., Ltd., et al. v. Molecular Rebar Design, LLC
IPR2025-00358

nanotubes. Nevertheless, the mean values of the viscosities obtained after the acid treatment can be very well differentiated and increases ~20% and 80%, in the case of the $MWCNT_{BMS}^{95}$ and $MWCNT_{FC}^{99}$, respectively. Under the previous assumptions, the oxidation reaction using $HNO_3$ unbundles more efficiently the $MWCNT_{FC}^{99}$ compared to the $MWCNT_{BMS}^{95}$. It is expected then that the low viscosity of the dispersion containing the acyl and alkyl chloride functionalized $MWCNT_{BMS}^{95}$ favors the grafting reaction more than the dispersion containing the acyl chloride functionalized $MWCNT_{FC}^{99}$. However, the relative low increase in viscosity of the dispersion of $MWCNT_{BMS}^{95}$ after the oxidation reaction might indicate that the disaggregation of these carbon nanotubes during the functionalization reactions is more difficult compared with the $MWCNT_{FC}^{99}$, as a consequence, the functionalization of the $MWCNT_{BMS}^{95}$ probably takes place rather on the surface of aggregates than on isolated carbon nanotubes.

Previous works have shown that noncovalent adsorption of poly(ethylene glycol) may occur during grafting.[21,61] Although the reactions have been performed at high concentration of the glycols and in the absence of solvent, the poly(ethylene glycol)s used have relative low molecular weights, and due to the thorough washing processes no or negligible adsorption should be present.[62] From the difference in weight loss between the MWCNTs after the acid treatment and after the *grafting onto* reaction of the glycols and the molecular weight of the glycols, one can estimate the concentration of hydroxyl groups ([OH]). This value is presented in the right axis in Figure 4. In the case of the $MWCNT_{BMS}^{95}$, the [OH] decreases dramatically when the glycol molecular weight increases. This suggests that even when the grafting content of the glycols increases with the molecular weight, the relative concentration of terminal hydroxyl group decreases. In the case of $MWCNT_{FC}^{99}$, the [OH] is lower compared with the $MWCNT_{BMS}^{95}$ and independent of the glycol used, in the range of molecular weights used in the present study. Then, the MWCNTs can be more easily dispersed in organic solvent because of the longer grafted chains, but have fewer functional groups available for the successive reactions.

The difference in [OH] between the $MWCNT_{BMS}^{95}$ and the $MWCNT_{FC}^{99}$ can be attributed to different factors. The concentration of acyl (or alkyl) chloride groups present on the $MWCNT_{BMS}^{95}$ and the $MWCNT_{FC}^{99}$ could be responsible for the difference of the grafting onto of the glycols, unfortunately, these differences are difficult to quantify using any of the existing characterization methods. The contour length of the MWCNTs estimated by the SFM measurements (Fig. 5) showed no marked difference between the dispersed nanoparticles that could infer any influence on the reaction efficiency.[63] However, the viscosity of the dispersion containing the MWCNTs seems to play a role on the grafting efficiency. The low viscosity of the dispersion of $MWCNT_{BMS}^{95}$ during the reaction might increase the accessibility of the hydroxyl groups to the acyl (or alkyl) chloride groups compared with the $MWCNT_{FC}^{99}$.

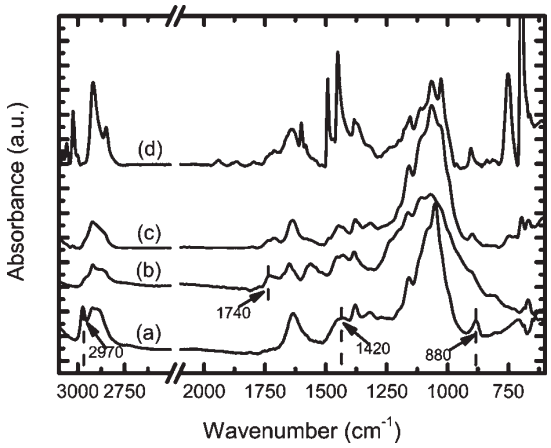


**FIGURE 6** Fourier transform infrared spectra of MWCNTs after different sequential modification steps (a) $PEG_{400}$ grafted $MWCNT_{FC}^{99}$, (b) $MWCNT_{FC}^{99}$-$Br^4$, (c) $PS_{44}^3MWCNT_{FC}^{99}$, and (d) $PS_{85}^{24}MWCNT_{FC}^{99}$.

A representative infrared spectrum of the MWCNTs after grafting of $PEG_{400}$ is presented in Figure 6. Even though the symmetric C—H stretching of the methylene groups is difficult to identify due to the alkyl groups of the MWCNTs, the C—H stretching deformations at ~1420 cm $^{1}$ and the C—O—C stretching deformation at 880 cm $^{1}$ are evident. These indicate the success of the reaction. An asymmetric C—H deformation is observed for this sample at 2970 cm $^{1}$, which is only observed clearly in MWCNTs modified with poly(ethylene glycol) of 400 g mol $^{1}$. The occurrence of any noncovalent interaction can be ruled out, since there is no evidence of the methylene groups related with nongrafted poly(ethylene glycol) at 2890 cm $^{1}$.[56]

**Esterification II: ATRP Initiator**

The infrared spectrum after anchoring the initiator groups for the controlled radical polymerization to the MWCNTs is also shown in Figure 6. The carboxylic acid stretching vibration located at 1740 cm $^{1}$ indicates the successful grafting of the initiator. Table 1 shows the initiator concentration estimated by elemental analysis. The reaction conditions were optimized to obtain comparable results of anchored initiator concentration [Br] for the MWCNTs from both used sources as a function of the 2BriBr concentration, as can be seen in Table 1 (entries 1 and 8). For this reason, the esterification reaction on the hydroxyl modified $MWCNT_{FC}^{99}$ was carried out at higher dilutions. Figure 7 shows the distribution of the average contour lengths of two MWCNTs with a comparable concentration of initiator. The length distribution of the MWCNTs shorter than ~1 $\mu$m does not appreciably change with respect to the values obtained after oxidation, however, longer carbon nanotubes could be found on the samples after the esterification, which confirms the assumption that the functionalization reaction helps to disaggregate the MWCNTs. In addition, longer carbon nanotubes were found in the sample $MWCNT_{FC}^{99}$-$Br^6$ than in the sample



10990488, 2010, 10, Downloaded from https://onlinelibrary.wiley.com/doi/10.1002/polb.21992 by Farrah Choudry - Test , Wiley Online Library on [21/12/2022]. See the Terms and Conditions (https://onlinelibrary.wiley.com/terms-and-conditions) on Wiley Online Library for rules of use; OA articles are governed by the applicable Creative Commons License



Samsung Ex. 1009, Page 7 of 12
Samsung Electronics Co., Ltd., et al. v. Molecular Rebar Design, LLC
IPR2025-00358

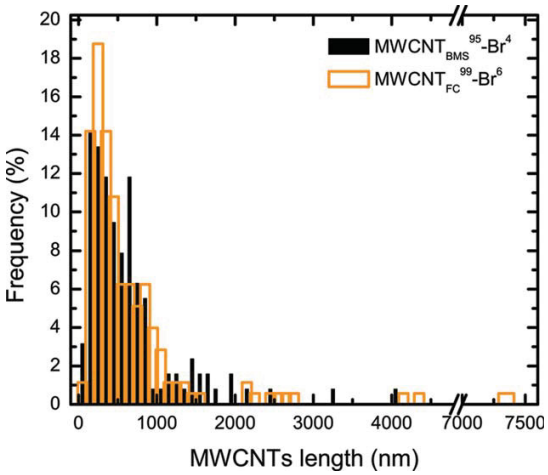


**FIGURE 7** Length distribution (nm) for MWCNTs after the grafting of the ATRP initiator. [Color figure can be viewed in the online issue, which is available at www.interscience.wiley.com.]

$MWCNT_{BMS}^{95}$-Br.[4] This could also be an indication that the $MWCNT_{FC}^{99}$ are effectively longer than the $MWCNT_{BMS}^{95}$ and that they are easier to disentangle due to the looseness of the aggregates.

In the case of the ethylene glycol modified MWCNTs, the anchored initiator concentrations shown in Table 1 for $MWCNT_{BMS}^{95}$ and $MWCNT_{FC}^{99}$ are comparable when low 2BriBr concentrations are used. By increasing the concentration of 2BriBr, the [Br] increased in both cases, though it is five times higher for the $MWCNT_{BMS}^{95}$ (0.62 mmol g $^{1}$) than for $MWCNT_{FC}^{99}$ (0.13 mmol g $^{1}$). To the authors' knowledge, the [Br] obtained for the $MWCNT_{BMS}^{95}$ under the described conditions is the highest value found on the grafting of initiator for surface initiated radical polymerizations on carbon nanotubes.[8,27,28,30,31,33,38,42,64,65]

The use of poly(ethylene glycol) spacers also affects the anchoring of the initiator. Under the same experimental conditions, the highest [Br] concentration is found on the MWCNTs grafted with $PEG_{200}$, followed by $PEG_{400}$ and EG. Two effects are involved in this behavior. On the one hand, it was previously discussed that the concentration of hydroxyl groups decreases if the molecular weight of the spacer increases (shown in Fig. 4) in the case of the $MWCNT_{BMS}^{95}$, whereas the concentration is rather low in the case of the $MWCNT_{FC}^{99}$. On the other hand, the stability of the carbon nanotube dispersions in organic solvents improves with the increment in spacer chain length, as well as the mobility of the hydroxyl end-groups. Therefore, as the molecular weight of the spacer increases, the esterification reaction takes place under conditions that resemble more those of a homogeneous reaction, which increases the feasibility of the reaction. Consequently, the observed tendency results from the competition between these two effects: the lower [Br] on the $PEG_{400}$ modified carbon nanotubes is assumed to be due to lower hydroxyl concentration, whereas the lower [Br] on the EG modified MWCNTs is attributed to the heterogeneity of the reaction.

### ATR Polymerization

Styrene (S) was chosen as a monomer for the *grafting from* the initiator anchored MWCNTs under controlled radical polymerization conditions. The results are summarized in Table 3. The decoration of carbon nanotubes and other substrates using this monomer has been well documented.[18,66–68] Styrene is able to solubilize its polymer, shows slower polymerization rate than other available monomers [i.e., meth (acrylates)],[69] and thermally polymerizes under the experimental conditions described.[43] These characteristics allow the study of the grafting without nonbonded initiators (free initiator), or deactivator (e.g., $CuBr_2$)[70] and with reduced quantity of solvent, which may complicate the analysis. In the styrene *grafting from* polymerization reactions, some free chains are always generated in solution, which promotes the termination in the reaction medium rather than within the active species attached to the substrate, and supports a controlled polymer growth in the sense that crosslinking between different nanoparticles will unlikely occur. This has been described previously on polymerization from silica nanostructures.[43,71,72]

The infrared spectra of polystyrene (PS) surface grafted MWCNTs under different reaction conditions are also shown in Figure 6. The bands corresponding to the polymer are clearly evident when the polymer content is over 70 wt %, for example, the = C—H stretching vibrations between 3100 and 3000 cm $^{1}$, the ring stretching vibration at ~1600 cm $^{1}$, the overtones between 2000 and 1660 cm $^{1}$, and the C—H out-of-plane vibration and ring out-of-plane deformation located at 760 cm $^{1}$ and 690 cm $^{1}$, respectively. Nuclear magnetic resonance ($^{1}$H NMR) measurements also support the presence of the grafted PS at the MWCNTs (results not shown). High polymer content is required also for the $^{1}$H NMR measurements, because the magnetization of the MWCNT promotes first the aggregation and then the sedimentation of the nanoparticles during the measurement.

Scanning electron micrographs are presented for a representative group of samples in Figure 8. Qualitatively, the PS grafted MWCNTs are similar, independent of the source ($MWCNT_{BMS}^{95}$ or $MWCNT_{FC}^{99}$). The scanning electron micrographs show that if the polymer content is below 50 wt %, the aspect ratio of the MWCNTs does not discern from the one of unmodified filler. When the polymer content is lower than ~20 wt % it is possible to analyze the sample without being sputtered, which indicates that the MWCNTs preserve their electrical conductivity characteristics after modification. This might represent an advantage in applications like conducting polymer films, where the preservation of the electrical conductivity in the nanofillers is required and a relatively good dispersion ensures a low MWCNTs percolation threshold in the nanocomposite. The samples with polymer content higher than 50 wt % present a more homogeneous structure, where the nanotubes look like they are embedded in



10990488, 2010, 10, Downloaded from https://onlinelibrary.wiley.com/doi/10.1002/polb.21992 by Farrah Choudry - Test , Wiley Online Library on [21/12/2022]. See the Terms and Conditions (https://onlinelibrary.wiley.com/terms-and-conditions) on Wiley Online Library for rules of use; OA articles are governed by the applicable Creative Commons License



Samsung Ex. 1009, Page 8 of 12
Samsung Electronics Co., Ltd., et al. v. Molecular Rebar Design, LLC
IPR2025-00358

**TABLE 3** Conditions and Polymer Content on the Styrene *Grafting from* Reaction on $MWCNT_{BMS}^{95}$ and $MWCNT_{FC}^{99}$

| Entry | Sample | Source | St[a] (wt %) | St[a] (mol %) | $t_{rxn}$ (h) | $f_{PS}$[b] (wt %) | $M_{n,TGA}$[c] (kg mol$^{-1}$) | $T_d$[d] (°C) |
|---|---|---|---|---|---|---|---|---|
| 1 | $PS_{19}{}^{3}MWCNT_{FC}{}^{99}$ | $MWCNT_{FC}{}^{99}$-$Br^{1}$ | 30 | 4,000 | 20.0 | 18.8 | 3 | 352 |
| 2 | $PS_{9}{}^{1}MWCNT_{FC}{}^{99}$ | $MWCNT_{FC}{}^{99}$-$Br^{2}$ | 30 | 2,200 | 20.1 | 9.0 | 1 | 272 |
| 3 | $PS_{11}{}^{1}MWCNT_{FC}{}^{99}$ | $MWCNT_{FC}{}^{99}$-$Br^{3}$ | 30 | 1,300 | 20.2 | 11.4 | 1 | 344 |
| 4 | $PS_{44}{}^{3}MWCNT_{FC}{}^{99}$ | $MWCNT_{FC}{}^{99}$-$Br^{4}$ | 30 | 1,200 | 20.1 | 44.1 | 3 | 375 |
| 5 | $PS_{85}{}^{24}MWCNT_{FC}{}^{99}$ | $MWCNT_{FC}{}^{99}$-$Br^{4}$ | 120 | 4,700 | 19.4 | 85.2 | 24 | 410 |
| 6 | $PS_{28}{}^{10}MWCNT_{FC}{}^{99}$ | $MWCNT_{FC}{}^{99}$-$Br^{5}$ | 30 | 6,700 | 23.7 | 28.1 | 10 | 361 |
| 7 | $PS_{22}{}^{2}MWCNT_{FC}{}^{99}$ | $MWCNT_{FC}{}^{99}$-$Br^{6}$ | 30 | 2,100 | 20.1 | 22.0 | 2 | 348 |
| 8 | $PS_{13}{}^{2}MWCNT_{FC}{}^{99}$ | $MWCNT_{FC}{}^{99}$-$Br^{7}$ | 30 | 3,800 | 20.0 | 12.8 | 2 | 335 |
| 9 | $PS_{23}{}^{4}MWCNT_{FC}{}^{99}$ | $MWCNT_{FC}{}^{99}$-$Br^{7}$ | 60 | 7,700 | 20.0 | 22.5 | 4 | 356 |
| 10 | $PS_{31}{}^{6}MWCNT_{FC}{}^{99}$ | $MWCNT_{FC}{}^{99}$-$Br^{7}$ | 120 | 15,400 | 20.1 | 30.6 | 6 | 371 |
| 11 | $PS_{32}{}^{6}MWCNT_{FC}{}^{99}$ | $MWCNT_{FC}{}^{99}$-$Br^{7}$ | 120 | 15,400 | 20.2 | 32.0 | 6 | 370 |
| 12 | $PS_{11}{}^{2}MWCNT_{FC}{}^{99}$ | $MWCNT_{FC}{}^{99}$-$Br^{7}$ | 30 | 3,800 | 20.2 | 11.1 | 2 | 331 |
| 13 | $PS_{34}{}^{7}MWCNT_{BMS}{}^{95}$ | $MWCNT_{BMS}{}^{95}$-$Br^{1}$ | 30 | 3,400 | 21.0 | 34.4 | 7 | 393 |
| 14 | $PS_{43}{}^{10}MWCNT_{BMS}{}^{95}$ | $MWCNT_{BMS}{}^{95}$-$Br^{1}$ | 30 | 3,400 | 26.0 | 43.4 | 10 | 394 |
| 15 | $PS_{47}{}^{11}MWCNT_{BMS}{}^{95}$ | $MWCNT_{BMS}{}^{95}$-$Br^{1}$ | 60 | 6,800 | 20.0 | 47.1 | 11 | 396 |
| 16 | $PS_{91}{}^{20}MWCNT_{BMS}{}^{95}$ | $MWCNT_{BMS}{}^{95}$-$Br^{2}$ | 30 | 430 | 20.0 | 91.3 | 20 | 420 |
| 17 | $PS_{85}{}^{9}MWCNT_{BMS}{}^{95}$ | $MWCNT_{BMS}{}^{95}$-$Br^{2}$ | 60 | 870 | 18.0 | 84.7 | 9 | 418 |
| 18 | $PS_{70}{}^{4}MWCNT_{BMS}{}^{95}$ | $MWCNT_{BMS}{}^{95}$-$Br^{2}$ | 60 | 870 | 7.0 | 70.4 | 4 | 406 |
| 19 | $PS_{86}{}^{17}MWCNT_{BMS}{}^{95}$ | $MWCNT_{BMS}{}^{95}$-$Br^{3}$ | 30 | 740 | 20.0 | 85.8 | 17 | 410 |
| 20 | $PS_{49}{}^{7}MWCNT_{BMS}{}^{95}$ | $MWCNT_{BMS}{}^{95}$-$Br^{4}$ | 30 | 2,900 | 20.1 | 49.1 | 7 | 387 |

[a] Weight and mole percent of styrene respect to the MWCNTs.
[b] Polystyrene grafting content.
[c] Average molecular weight of the grafted polystyrene, calculated from TGA.[28]
[d] Decomposition onset temperature calculated from TGA data.

polymer. This effect has been previously observed by other groups.[31,42]

From the transmission electron micrographs (shown as inserts in Fig. 8) one could assume that the graphitic-like structure of the nanotubes is preserved after all the functionalization reactions. The grafting of polymer takes place along the MWCNTs, not just on their tips, where the highest initiator concentration is supposed to be due to a major concentration of defects. However, as previously discussed, the infrared analysis on the pristine MWCNTs shows that defects are present along the structure. These potentially reactive locations enable the distribution of initiator groups along the MWCNTs.

The quantity of polymer grafted on the MWCNTs from both sources could be controlled by adjusting the weight ratio between the monomer and the nanofiller as a function of the initiator concentration. The results are summarized in Table 3. The weight ratios used in this work are comparable to the experimental conditions presented in other studies,[40,42] although there is lack of agreement throughout the literature.[22,30,31]

The results presented in Table 3 show that, in general, higher polymer content is obtained for the initiator anchored $MWCNT_{BMS}{}^{95}$ than for $MWCNT_{FC}{}^{99}$, when the grafting takes place under similar reaction conditions. The observed discrepancies are believed to depend on the intrinsic characteristics of the carbon nanotubes used here. For example, in the case of the samples $PS_{19}{}^{3}MWCNT_{FC}{}^{99}$ and $PS_{34}{}^{7}MWCNT_{BMS}{}^{95}$ (entries 1 and 13), the polymer content for $MWCNT_{BMS}{}^{95}$ is almost twice of the one obtained for $MWCNT_{FC}{}^{99}$ under comparable reaction conditions. The interplay of two factors explains this difference. First, the distribution of anchored initiator along the MWCNTs varies with the location of the structural defects, which is predetermined from the carbon nanotubes synthesis. If the initiator moieties are close to each other, coupling or deactivation reactions will compete with the propagation of the living chain. This could be related with the critical conversion of coupling (CCC),[8] where not just the electronic properties of the carbon nanotube may affect the polymerization, but also the location of the growing chain could induce coupling reactions. Second, as discussed before, the viscosity of the dispersions containing $MWCNT_{BMS}{}^{95}$ is lower than the dispersion prepared with the $MWCNT_{FC}{}^{99}$ due to the presence of relative compact aggregates and shorter carbon nanotubes. For this reason, the overall polymerization rate could be higher or a major reaction yield could be reached with the $MWCNT_{BMS}{}^{95}$-Br.

If the monomer to MWCNT weight ratio is kept constant, the amount of grafted polymer increases with the concentration of initiator anchored on $MWCNT_{BMS}{}^{95}$ and decreases for the initiator anchored on $MWCNT_{FC}{}^{99}$. The competition between polymer conversion, initiator concentration, and dispersion of the MWCNTs might explain these results. Short polymer



10990488, 2010, 10, Downloaded from https://onlinelibrary.wiley.com/doi/10.1002/polb.21992 by Farrah Choudry - Test , Wiley Online Library on [21/12/2022]. See the Terms and Conditions (https://onlinelibrary.wiley.com/terms-and-conditions) on Wiley Online Library for rules of use; OA articles are governed by the applicable Creative Commons License



Samsung Ex. 1009, Page 9 of 12
Samsung Electronics Co., Ltd., et al. v. Molecular Rebar Design, LLC
IPR2025-00358

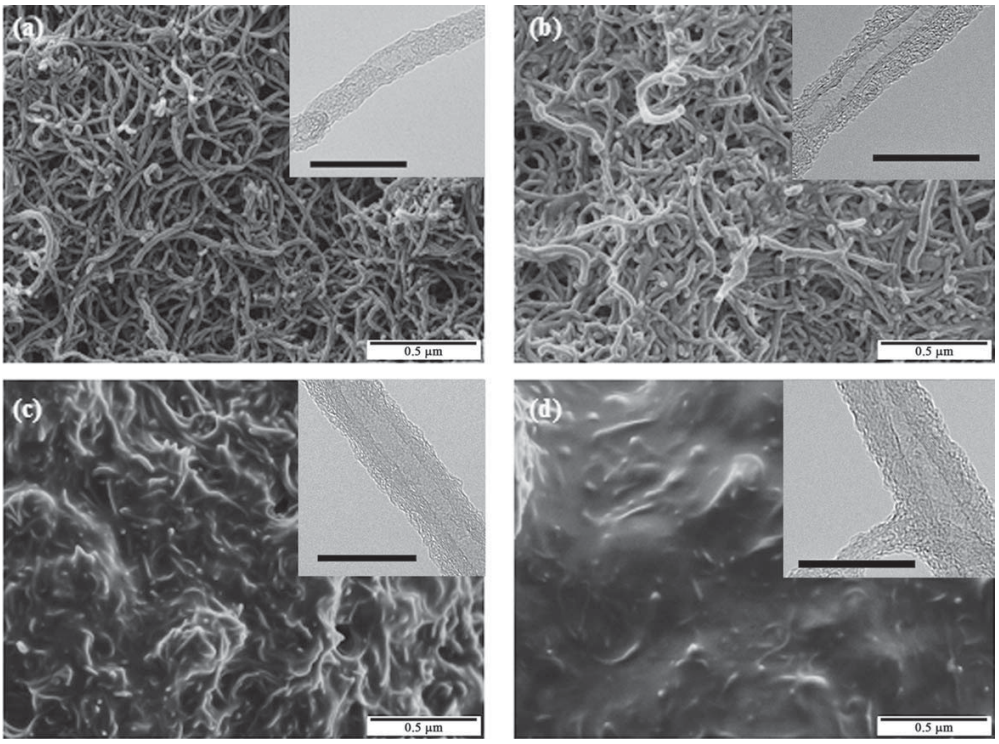


**FIGURE 8** Scanning and transmission (inserts) electron micrographs of MWCNT grafted with PS, synthesized under the conditions indicated in Table 3. (a) $PS_9{}^{1}MWCNT_{FC}{}^{99}$, (b) $PS_{44}{}^{3}MWCNT_{FC}{}^{99}$, (c) $PS_{70}{}^{4}MWCNT_{BMS}{}^{95}$, and (d) $PS_{91}{}^{20}MWCNT_{BMS}{}^{95}$. TEM scale bar = 20 nm.

chains grafted from apparent shorter and more aggregated carbon nanotubes increase less dramatically the viscosity during the grafting from polymerization than apparent longer and less aggregated carbon nanotubes, as is the case of $MWCNT_{FC}{}^{99}$-Br. As a result, the grafting reactions on $MWCNT_{BMS}{}^{95}$-Br take place probably for prolonged times before the increase in viscosity decreases the propagation rate of the reaction, and this results in higher polymer contents. This behavior has been previously observed in the literature, although a clear correlation with the results presented here is not possible since no data is given regarding the length of the carbon nanotubes.[42]

The dispersion plays an important role on all the carbon nanotubes functionalization reactions. Before grafting, both $MWCNT_{BMS}{}^{95}$-Br and $MWCNT_{FC}{}^{99}$-Br are dispersed in the monomer. To obtain optically homogeneous carbon nanotube dispersions before the start of the polymerization, the minimum feasible monomer-to-nanofiller weight ratio found was 30 to 1; lower ratios lead to highly viscous dispersions before the start of the reaction. In the case of the $MWCNT_{FC}{}^{99}$, the variation of the monomer-to-nanofiller weight ratio influences the content of grafted polymer. For example, increasing four times the monomer concentration with respect to $MWCNT_{FC}{}^{99}$-Br[7] (Table 3, Entries 8–11) the polystyrene weight fraction increases ~2.4 times. The low solution viscosity due to the high concentration of monomer at the beginning of the reaction enhances the access of the monomer to the propagating radical and extends the reaction time. The carbon nanotubes dispersion improves during the polymerization reaction due to the growing chains, but the viscosity rises due to the monomer consumption. Then, the reaction will be controlled until the dispersion is hindered by the monomer consumption, the surface confinement between nanotubes will limit the propagation and coupling or disproportions might end the reaction. As the conversion of monomer advances, the viscosity rises and promotes the filler reaggregation, so that the deactivation of the growing radical is favored (as described above).

A common trend on the MWCNTs from both sources after ATRP reactions is the increase in grafted polymer content with the monomer concentration. The increase in polymer content with the monomer concentration has been also reported on MWCNTs[31] and other confined systems.[71] These observations can be correlated to the transmission electron micrographs (inserts in Fig. 8). If one assumes that the distribution of initiator moieties is homogeneous along the surface on both MWCNT sources, the polymer layer is relatively thinner for the $PS_{44}{}^{3}MWCNT_{FC}{}^{99}$ than for the sample $PS_{91}{}^{20}MWCNT_{BMS}{}^{95}$. This is in agreement with other systems, where the polymer grafting depends on the



10990488, 2010, 10, Downloaded from https://onlinelibrary.wiley.com/doi/10.1002/polb.21992 by Farrah Choudry - Test , Wiley Online Library on [21/12/2022]. See the Terms and Conditions (https://onlinelibrary.wiley.com/terms-and-conditions) on Wiley Online Library for rules of use; OA articles are governed by the applicable Creative Commons License



Samsung Ex. 1009, Page 10 of 12
Samsung Electronics Co., Ltd., et al. v. Molecular Rebar Design, LLC
IPR2025-00358

nanoparticle surface area and its influence on the polymerization kinetics.[43]

Another possibility to control the polystyrene content in the $MWCNT_{FC}^{99}$ is by varying the length of the glycol spacer. As can be observed in Table 3, for comparable monomer to $MWCNT_{FC}^{99}$ weight fractions and initiator concentration, the polystyrene grafting content doubles when ethylene glycol and $PEG_{400}$ are compared ($PS_9{}^1MWCNT_{FC}^{99}$ and $PS_{22}{}^2MWCNT_{FC}^{99}$) and increases four times when $PEG_{200}$ is compared against $PEG_{400}$ ($PS_{11}{}^1MWCNT_{FC}^{99}$ and $PS_{44}{}^3MWCNT_{FC}^{99}$). A polymer content over 80 wt % can be obtained with the $MWCNT_{FC}^{99}$ by choosing the right combination between glycol spacer, initiator concentration, and monomer to carbon nanotube ratio (e.g., $PS_{85}{}^{24}MWCNT_{FC}^{99}$, entry 5 in Table 3). From the obtained results one can deduce that the $PEG_{400}$ chain length promotes a more stable dispersion and lower the viscosity of the reactions compared to the other glycol spacers used, which increase the polymer grafting weight content through the increase in the polymerization rate or the increase of the yield during the time of the polymerizations.

## CONCLUSIONS

Two commercially available MWCNTs were grafted with polystyrene after successive functionalization reactions. The *grafting from* polymerization of styrene was performed under atom transfer radical polymerization conditions. The purity and the dimension of the MWCNTs influence the grafted polystyrene content. The MWCNT with relative tighter aggregates and with apparent shorter length ($MWCNT_{BMS}^{95}$) showed a higher polystyrene weight content than the relative longer, less aggregated carbon nanotubes ($MWCNT_{FC}^{99}$), with comparable initiator concentrations. The presence of tight aggregates and shorter nanotubes decreases the viscosity of the dispersion during the functionalization reactions, which may enhance the propagation of the growing polymer chain before the polymerization slows down due to high monomer conversion. However, higher polymer contents can be achieved with the $MWCNT_{FC}^{99}$ with the right combination of poly(ethylene glycol) spacer, concentration of the anchored initiator, and monomer to carbon nanotube weight ratio.

Baytubes® were kindly supplied by Bayer MaterialScience. The authors thank Clarissa Abetz for TEM and Karen-Marita Prause for SEM investigations. J.A. acknowledges DAAD-HGF fellowship. The authors acknowledge financial support by the seventh Framework Program of the European Commission [HARCANA (NMP3-LA-2008-213277)].

## REFERENCES AND NOTES

**1** Moniruzzaman, M.; Winey, K. I. Macromolecules 2006, 39, 5194–5205.

**2** Iijima, S. Nature 1991, 354, 56–58.

**3** Monthioux, M.; Kuznetsov, V. L. Carbon 2006, 44, 1621–1623.

**4** Gojny, F. H.; Schulte, K. Compos Sci Technol 2004, 64, 2303–2308.

**5** Sandler, J. K. W.; Kirk, J. E.; Kinloch, I. A.; Shaffer, M. S. P.; Windle, A. H. Polymer 2003, 44, 5893–5899.

**6** Shi, Q.; Yang, D.; Su, Y.; Li, J.; Jiang, Z.; Jiang, Y.; Yuan, W. J. Nanopart Res 2007, 9, 1205–1210.

**7** Kumar, N. A.; Ganapathy, H. S.; Kim, J. S.; Jeong, Y. S.; Jeong, Y. T. Eur Polym J 2008, 44, 579–586.

**8** Gao, C.; Muthukrishnan, S.; Li, W.; Yuan, J.; Xu, Y.; Muller, A. H. E. Macromolecules 2007, 40, 1803–1815.

**9** Richard, C.; Balavoine, F.; Schultz, P.; Ebbesen, T. W.; Mioskowski, C. Science 2003, 300, 775–778.

**10** Poland, C. A.; Duffin, R.; Kinloch, I.; Maynard, A.; Wallace, W. A. H.; Seaton, A.; Stone, V.; Brown, S.; MacNee, W.; Donaldson, K. Nat Nanotechnol 2008, 3, 423–428.

**11** Kane, A. B.; Hurt, R. H. Nat Nanotechnol 2008, 3, 378–379.

**12** Rausch, L. J.; Bisinger, E. C.; Sharma, A. Regul Toxicol Pharm 2004, 40, 28–41.

**13** Schipper, M. L.; Nakayama-Ratchford, N.; Davis, C. R.; Kam, N. W. S.; Chu, P.; Liu, Z.; Sun, X.; Dai, H.; Gambhir, S. S. Nat Nanotechnol 2008, 3, 216–221.

**14** Gojny, F. H.; Wichmann, M. H. G.; Fiedler, B.; Kinloch, I. A.; Bauhofer, W.; Windle, A. H.; Schulte, K. Polymer 2006, 47, 2036–2045.

**15** Sandler, J.; Shaffer, M. S. P.; Prasse, T.; Bauhofer, W.; Schulte, K.; Windle, A. H. Polymer 1999, 40, 5967–5971.

**16** Sandler, J. K. W.; Pegel, S.; Cadek, M.; Gojny, F.; van Es, M.; Lohmar, J.; Blau, W. J.; Schulte, K.; Windle, A. H.; Shaffer, M. S. P. Polymer 2004, 45, 2001–2015.

**17** Shim, M.; Shi Kam, N. W.; Chen, R. J.; Li, Y.; Dai, H. Nano Lett 2002, 2, 285–288.

**18** Tasis, D.; Tagmatarchis, N.; Bianco, A.; Prato, M. Chem Rev 2006, 106, 1105–1136.

**19** Sung, J.; Park, J. M.; Choi, U. H.; Huh, J.; Jung, B.; Min, B. G.; Ahn, C. H.; Park, C. Macromol Rapid Commun 2007, 28, 176–182.

**20** Hill, D. E.; Lin, Y.; Rao, A. M.; Allard, L. F.; Sun, Y. P. Macromolecules 2002, 35, 9466–9471.

**21** Baskaran, D.; Mays, J. W.; Bratcher, M. S. Polymer 2005, 46, 5050–5057.

**22** Chang, J. H.; Lee, Y. W.; Kim, B. G.; Kim, H.-K.; Choi, I. S.; Paik, H.-J. Compos Interface 2007, 14, 493–504.

**23** Cheng, B.; Li, Y.; Shen, C. Polym Prepr (Am Chem Soc Div Polym Chem) 2004, 45, 653–654.

**24** Chochos, C. L.; Stefopoulos, A. A.; Campidelli, S.; Prato, M.; Gregoriou, V. G.; Kallitsis, J. K. Macromolecules 2008, 41, 1825–1830.

**25** Choi, J. H.; Oh, S. B.; Chang, J.; Kim, I.; Ha, C.-S.; Kim, B. G.; Han, J. H.; Joo, S.-W.; Kim, G.-H.; Paik, H.-j. Polym Bull 2005, 55, 173–179.

**26** Fragneaud, B.; Masenelli-Varlot, K.; Gonzalez-Montiel, A.; Terrones, M.; Cavaillé, J.-Y. Chem Phys Lett 2006, 419, 567–573.



10990488, 2010, 10, Downloaded from https://onlinelibrary.wiley.com/doi/10.1002/polb.21992 by Farrah Choudry - Test , Wiley Online Library on [21/12/2022]. See the Terms and Conditions (https://onlinelibrary.wiley.com/terms-and-conditions) on Wiley Online Library for rules of use; OA articles are governed by the applicable Creative Commons License



Samsung Ex. 1009, Page 11 of 12
Samsung Electronics Co., Ltd., et al. v. Molecular Rebar Design, LLC
IPR2025-00358

**27** Gao, C.; Li, W.; Morimoto, H.; Nagaoka, Y.; Maekawa, T. J Phys Chem B 2006, 110, 7213–7220.

**28** Gao, C.; Vo, C. D.; Jin, Y. Z.; Li, W.; Armes, S. P. Macromolecules 2005, 38, 8634–8648.

**29** Hong, C. Y.; You, Y. Z.; Wu, D.; Li, Y.; Pan, C. Y. Macromolecules 2005, 38, 2606–2611.

**30** Kong, H.; Gao, C.; Yan, D. J Am Chem Soc 2004, 126, 412–413.

**31** Kong, H.; Gao, C.; Yan, D. Macromolecules 2004, 37, 4022–4030.

**32** Kong, H.; Gao, C.; Yan, D. J Mater Chem 2004, 14, 1401–1405.

**33** Kong, H.; Luo, P.; Gao, C.; Yan, D. Polymer 2005, 46, 2472–2485.

**34** Lei, Z.; Wei, X.; Zhang, L.; Bi, S. Colloid Surf A 2008, 324, 131–136.

**35** Li, W.; Gao, C.; Qian, H.; Ren, J.; Yan, D. J Mater Chem 2006, 16, 1852–1859.

**36** Liu, Y. L.; Chen, W. H. Macromolecules 2007, 40, 8881–8886.

**37** Matrab, T.; Chancolon, J.; L'Hermite, M. M.; Rouzaud, J.-N.; Deniau, G.; Boudou, J.-P.; Chehimi, M. M.; Delamar, M. Colloid Surf A 2006, 287, 217–221.

**38** Qin, S.; Qin, D.; Ford, W. T.; Resasco, D. E.; Herrera, J. E. J Am Chem Soc 2004, 126, 170–176.

**39** Qin, S.; Qin, D.; Ford, W. T.; Resasco, D. E.; Herrera, J. E. Macromolecules 2004, 37, 752–757.

**40** Wu, H.-X.; Tong, R.; Qiu, X.-Q.; Yang, H.-F.; Lin, Y.-H.; Cai, R.-F.; Qian, S.-X. Carbon 2007, 45, 152–159.

**41** Xiao, Q.; He, S.; Liu, L.; Guo, X.; Shi, K.; Du, Z.; Zhang, B. Compos Sci Technol 2008, 68, 321–328.

**42** Baskaran, D.; Mays, J. W.; Bratcher, M. S. Angew Chem Int Ed 2004, 43, 2138–2142.

**43** von Werne, T.; Patten, T. E. J Am Chem Soc 2001, 123, 7497–7505.

**44** Huang, C.; Tassone, T.; Woodberry, K.; Sunday, D.; Green, D. L. Langmuir 2009, 25, 13351–13360.

**45** Wang, T.-L.; Tseng, C.-G. J Appl Polym Sci 2007, 105, 1642–1650.

**46** Osswald, S.; Havel, M.; Gogotsi, Y. J Raman Spectrosc 2007, 38, 728–736.

**47** Shanmugharaj, A. M.; Bae, J. H.; Lee, K. Y.; Noh, W. H.; Lee, S. H.; Ryu, S. H. Compos Sci Technol 2007, 67, 1813–1822.

**48** Chen, Q.; Xu, R.; Yu, D. Polymer 2006, 47, 7711–7719.

**49** Sun, L.; Yang, J.-T.; Lin, G.-Y.; Zhong, M.-Q. Mater Lett 2007, 61, 3963–3966.

**50** Zhang, J.; Zou, H.; Qing, Q.; Yang, Y.; Li, Q.; Liu, Z.; Guo, X.; Du, Z. J Phys Chem B 2003, 107, 3712–3718.

**51** Xu, D.; Liu, H.; Yang, L.; Wang, Z. Carbon 2006, 44, 3226–3231.

**52** Wu, C.-S. J Appl Polym Sci 2007, 104, 1328–1337.

**53** Zhang, X.; Deng, C.; Xu, R.; Wang, D. J Mater Sci 2007, 42, 8377–8380.

**54** Datsyuk, V.; Kalyva, M.; Papagelis, K.; Parthenios, J.; Tasis, D.; Siokou, A.; Kallitsis, I.; Galiotis, C. Carbon 2008, 46, 833–840.

**55** Xia, W.; Wang, Y.; Bergsträßer, R.; Kundu, S.; Muhler, M. Appl Surf Sci 2007, 254, 247–250.

**56** Baskaran, D.; Mays, J. W.; Bratcher, M. S. Chem Mater 2005, 17, 3389–3397.

**57** Forrest, G. A.; Alexander, A. J. J Phys Chem C 2007, 111, 10792–10798.

**58** Peng, F.; Zhang, L.; Wang, H.; Lv, P.; Yu, H. Carbon 2005, 43, 2405–2408.

**59** Ziegler, K. J.; Gu, Z.; Peng, H.; Flor, E. L.; Hauge, R. H.; Smalley, R. E. J Am Chem Soc 2005, 127, 1541–1547.

**60** Breza, M. Chem Phys 2006, 330, 224–230.

**61** Sano, M.; Kamino, A.; Okamura, J.; Shinkai, S. Langmuir 2001, 17, 5125–5128.

**62** Liu, Y.-X.; Du, Z.-J.; Li, Y.; Zhang, C.; Li, C.-J.; Yang, X.-P.; Li, H.-Q. J Polym Sci Part A: Polym Chem 2006, 44, 6880–6887.

**63** Lin, Y.; Taylor, S.; Huang, W.; Sun, Y. P. J Phys Chem B 2003, 107, 914–919.

**64** Yao, Z.; Braidy, N.; Botton, G. A.; Adronov, A. J Am Chem Soc 2003, 125, 16015–16024.

**65** Fan, D.-Q.; He, J.-P.; Tang, W.; Xu, J.-T.; Yang, Y.-L. Eur Polym J 2007, 43, 26–34.

**66** Lan, Q.; Francis, L. F.; Bates, F. S. J Polym Sci Part B: Polym Phys 2007, 45, 2284–2299.

**67** El Harrak, A.; Carrot, G.; Oberdisse, J.; Jestin, J.; Boué, F. Polymer 2005, 46, 1095–1104.

**68** De Falco, A.; Fascio, M. L.; Lamanna, M. E.; Corcuera, M. A.; Mondragon, I.; Rubiolo, G. H.; D'Accorso, N. B.; Goyanes, S. Phys B: Condens Matter 2009, 404, 2780–2783.

**69** Matyjaszewski, K.; Xia, J. Chem Rev 2001, 101, 2921–2990.

**70** Matyjaszewski, K.; Miller, P. J.; Shukla, N.; Immaraporn, B.; Gelman, A.; Luokala, B. B.; Siclovan, T. M.; Kickelbick, G.; Vallant, T.; Hoffmann, H.; Pakula, T. Macromolecules 1999, 32, 8716–8724.

**71** Moreno, J.; Sherrington, D. C. Chem Mater 2008, 20, 4468–4474.

**72** Audouin, F.; Blas, H.; Pasetto, P.; Beaunier, P.; Boissière, C.; Sanchez, C.; Save, M.; Charleux, B. Macromol Rapid Commun 2008, 29, 914–921.



10990488, 2010, 10, Downloaded from https://onlinelibrary.wiley.com/doi/10.1002/polb.21992 by Farrah Choudry - Test , Wiley Online Library on [21/12/2022]. See the Terms and Conditions (https://onlinelibrary.wiley.com/terms-and-conditions) on Wiley Online Library for rules of use; OA articles are governed by the applicable Creative Commons License



Samsung Ex. 1009, Page 12 of 12
Samsung Electronics Co., Ltd., et al. v. Molecular Rebar Design, LLC
IPR2025-00358